UNSTEADY BEHAVIOR OF A SIMULATED LNG VAPOR CLOUD SUDDENLY RELEASED INTO A WIND-TUNNEL BOUNDARY LAYER

by

Robert N. Meroney*

Paper Presented

AMERICAN GAS ASSOCIATION
TRANSMISSION CONFERENCE

Seattle, Washington
May 2-4, 1983

* Professor, Fluid Mechanics and Wind Engineering Program Civil Engineering Department, Colorado State University, Fort Collins

CEP82-83RNM17

UNSTEADY BEHAVIOR OF A SIMULATED LNG VAPOR CLOUD SUDDENLY RELEASED INTO A WIND-TUNNEL BOUNDARY LAYER

R. N. Meroney
Wind Engineering and Fluid Mechanics
Department of Civil Engineering
Colorado State University
Fort Collins, CO, U.S.A.

ABSTRACT

The behavior of dense gas volumes emitted suddenly into a simulated atmospheric boundary layer are used to calibrate a numerical volume-integrated box model. The box model which includes relations to account for surface heat transfer and atmospheric humidity is compared to field releases of Freon and Liquid Natural Gas.

1.0 INTRODUCTION

Sudden release of a dense gas near the ground is accompanied by horizontal spreading caused by gravitational forces. Such clouds will drift downwind from the source location at ground level, providing an opportunity for ignition if the gas is flammable or perhaps for acute toxic effect to life in its path. When the buoyancy forces are large they tend to dominate cloud shape, inhibit advection by the wind, and suppress dispersion by atmospheric turbulence.

There now exist a number of well-documented field studies of the behavior of dense gas clouds dispersing over the ground. Puttock, Blackmore and Colenbrander (1982) review some 295 experiments performed over land or water as of 1981. Release gases include ammonia, Freon, LNG, oxygen, and propane. Liquid volumes released range from 0.04 to 198 cubic meters. Among the most well documented are the recent Health and Safety Executive (HSE) Freon tests at Porton, U.K., the Department of Energy China Lake "Burro" series spills of LNG, and the Shell Map-

lin Sands, U.K. spills of propane and LNG (Picknett, (1978); Koopman et al., (1982); and Puttock et al., (1982)). Laboratory experience with dense gases is summarized by Meroney (1982). Except for a few laboratory experiments all tests were single replication measurements of a unique combination of spill, atmospheric boundary layer, and surface characteristics. Previous analytical or numerical models calibrated from these data sets suffer from using data which were single realizations from some unknown probability distribution (pdf) to stipulate adjustable constants in models designed to predict mean behavior.

This paper considers the results of a set of systematic and replicated wind-tunnel experiments performed to examine the behavior of dense-gas clouds and plumes during periods of gravity-spread/air-entrainment dominance. An instantaneous-source box model is presented which includes the influence of surface heat transfer and atmospheric humidity. The model is compared to independent field measurements of Freon and LNG vapor behavior without any additional modification or revision of model constants.

2.0 BOX MODELS AND THEIR LIMITATIONS

Consider a dense cloud which is instantaneously released as a cylindrical box of radius, R_i, and height, H_i, that undergoes a slumping motion in which R increases with time. As the motion proceeds one may assume the box mixes with ambient air, but maintains uniform properties internally. The radial velocity is assumed to vary linearly from zero at the center to a maximum at the outer edge of the cloud. Entrainment may occur over the upper cloud surface and at the front edge. Model details are contained in Appendix A of Meroney and Lohmeyer [ref. 12].

Frontal spread velocities are calculated from a modified version of the total energy budget equation suggested by van Ulden [ref. 13].

Dilution of the gas cloud occurs by entrainment across the upper cloud surface and the frontal area. These entrainment rates are adjusted to account for stratification-modified gravity spread rate and background turbulence. Finally, although some models propose to relate drift distance to drift time by a normal wind speed (i.e., $x \simeq u_R t$, where u_R is a reference velocity), the current calculations use a momentum entrainment equation.

The final equations developed were nondimensionalized with respect to time and space scales equal to $T = V_i^{1/6}(g_i')^{-1/2}$ and $L = V_i^{1/3}$ respectively where $g_i' = g(SG_i - 1)$. Nondimensional variables are indicated by a superscript star (*). The final expressions used are

Energy Equation:

$$\frac{du_g^*}{dt^*} = \left(\frac{2}{\pi} \frac{1}{R^{*3}} \left(\frac{\Delta\rho}{\Delta\rho_i}\right) V^* - \frac{u_r^* u_g^*}{R^*} - \frac{u_z^* u_g^*}{2H^*} \right) \rho^{*-1} - 2\beta_1 \frac{u_g^{*2}}{R^*} \tag{1}$$

Radial Growth Equation:

$$\frac{dR^*}{dt^*} = u_g^* \text{, but never less than} \tag{2a}$$

$$\frac{dR^*}{dt^*} = \frac{\alpha_7}{Ri_*^{1/2}} \tag{2b}$$

Dilution Equation:

$$\frac{d(\chi^{-1})}{dt^*} = [\pi R^{*2} u_z^* + 2\pi R^* H^* u_r^*](1 - \theta) \tag{3}$$

Enthalpy Equation:

$$\frac{dE^*}{dt^*} = \pi R^{*2} h_s^* T^* + (HS)\ (LHTS)\ (1 - \beta)\frac{d(\chi^{-1})}{dt^*}[\omega_{\phi,Ta} - \omega_{100,T} - F(T)(1 - \chi)\chi] \tag{4}$$

Momentum Equation:

$$\frac{dM^*}{dt^*} = \frac{u_a^*}{(1-\theta)} \frac{d(\chi^{-1})}{dt^*} - \rho^* \pi R^{*2} \left(\frac{C_f}{2}\right) u_x^{*2} \tag{5}$$

Advection Equation:

$$\frac{d\chi^*}{dt^*} = u_x^* + u_g^* \tag{6}$$

Algebraic Relations and State Equations:

$$E^* = -\frac{1}{\chi} \left(\frac{1 + \chi s^*}{1 + s^*}\right) T^* \tag{7}$$

$$u_x^* = \frac{M^*}{\rho^* \pi R^{*2} H^*} \tag{8}$$

$$\chi = \frac{1}{V^*} \frac{(1 - T^*\theta)}{(1-\theta)} \qquad \rho^* = \frac{\chi + (1-\chi)(1-\beta)}{(1-\beta)(1 - T^*\theta)} \tag{9a,9b}$$

$$u_a^* = \frac{1}{k} Ri_*^{-1/2} \ln(H^*/z_o^* + 1) \tag{10}$$

$$h_s^* = 0.32 \left(\frac{Gr}{Re_*^3 Pr}\right)^{1/2} Ri_*^{-1/2} \frac{(1 + \chi s^*)}{(1 + s^*)} \frac{(1-\theta)}{(1 - T^*\theta)} T^{*1/2} \tag{11}$$

Entrainment Relations:

$$u_r^* = c_r u_g^* \tag{12a}$$

$$u_z^* = c_z u_g^* + \frac{\alpha_4 w^*}{\frac{\alpha_4}{\alpha_6} + \frac{Ri_*}{\rho_* \pi R^{*2}}} \tag{12b}$$

$$w^{*2} = \alpha_3^2 / Ri_* + \alpha_2^2 \left[\frac{Gr}{Re^2} \frac{(1 + s^*)(1 - T^*\theta)}{(1 + \chi s^*)(1-\theta)} H^* h_s^* T^*\right]^{2/3} \tag{12c}$$

where

$$
\left.
\begin{aligned}
Ri_* &= (g_i')V_i^{1/3}/u_*^2, & s^* &= \frac{c^*_{p_i}}{c^*_{p_a}} - 1 \\
Re_* &= \frac{\rho_a V_i^{1/3} u_*}{\mu_a}, & \theta &= 1 - \frac{T_i}{T_a} \\
Re &= Re_* Ri_*^{1/2}, & \beta &= 1 - \frac{M_a}{M_i} \\
Gr &= \frac{g\beta(T_a - T_i)V_i}{\nu_a^2},
\end{aligned}
\right\} \quad (13)
$$

The above relations include the effects of gas mixture on properties, whereas the influence of humidity during condensation and re-evaporation is included in the enthalpy conservation Equation (4). The Boussinesq assumption was not made during the development of these expressions. The dimensionless heat transfer coefficient (Equation (11)) is based on the bulk transfer coefficient for mixed free and forced convection in the atmosphere recommended by Leovy (1969). LHTS is a dimensionless heat of vaporization for water vapor. F(T) is also from the humidity equation of state. (HS) is the Heavyside Operator for $T \lesseqgtr T_{dewpoint}$.

Constants found to fit the wind tunnel data most satisfactorily are $c_r = c_z = 0.1$, $\beta_1 = 0.9$, $\alpha_2 = 0.5$, $\alpha_3 = 1.0$, $\alpha_4 = 2.5$, $\alpha_6 = 0.30$, $\alpha_7 = 3.5$, and $k = 0.4$. Equations (1) thru (6) were integrated by a fourth-order Runga-Kutta scheme. Note that the cloud dispersion is only a function of initial cloud geometry (i.e., R_i/H_i ratio), Richardson number, Ri_*, Grashof number, Gr, surface roughness length, z_o^*, and initial specific gravity.

3.0 EXPERIMENTAL CONFIGURATION

An experiment was designed to examine the dispersion of instantaneous volumes of dense gas released at ground level in a wind tunnel capable of simulating the atmospheric boundary layer. The gases are

released as initially half cylindrical clouds and the concentrations were monitored by an aspirated-hot-wire katherometer.

3.1 Wind Tunnel and Source Generation Equipment

The open circuit wind tunnel used had a test section 0.5 m high, 1.5 m wide, and 5 m long. At the tunnel entrance was a dense honeycomb and a vortex spire/barrier flow-conditioner arrangement which produced a 30 cm deep turbulent shear layer which reached equilibrium and remained stationary over the final 3 meters of the test section. A 14 cm x 16 cm x 12 cm deep container of water was maintained flush to the test section floor 2.5 meters from the entrance as noted in Figure 1. The rectangular box contained an apparatus to fill a half cylinder cup with dense gas, to raise the filled cylinder above the water surface until it stood exposed to the wind, but isolated by a water seal, and to suddenly rotate the horizontal cylinder about its axis, leaving a volume of dense gas almost motionless above the water surface. The cup rotated 180 in less than 1/20 second. A small magnet on the cup activated a reed switch which provided a voltage pulse to timing instrumentation.

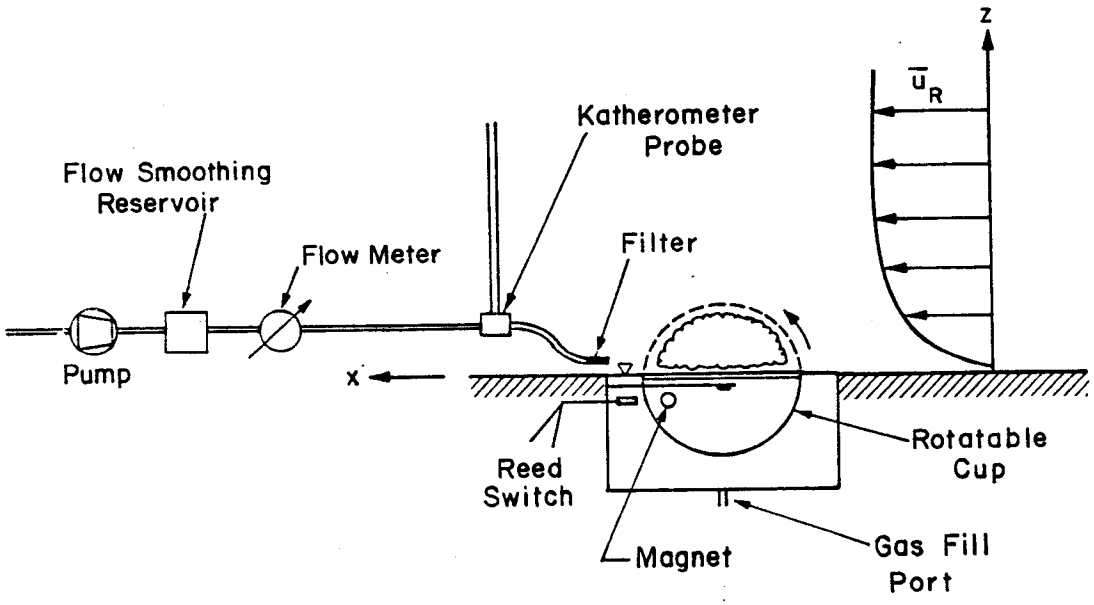

Figure 1. Experimental Configuration

3.2 Concentration Measurements

Dense gas concentrations were measured with an aspirated-hot-film anemometer (katherometer) constructed from a DISA 55E07 mass flow transducer. The aspiration velocity at the 1 mm diameter probe tip was set at less than 0.1 m/sec to assure approximately isokinetic sampling of the plume. A fiber filter was present at the probe tip to reduce system sensitivity to pressure perturbations during shear flow measurements. All tests were corrected for a slight time lag required for the sample to travel through the probe to the detection wire. Extensive tests indicate such a probe has a flat frequency response to 150 Hertz, concentration sensitivity to 0.10 percent, and resolution within ±5 percent of a measurement (Meroney, Neff, and Cermak (1978)). Since the probe is subject to drift and temperature effects it was recalibrated frequently. No significant deviations were detected.

During each realization of a volume release the katherometer response was registered on a chart recorder. Each sample point was recorded a minimum of five times. Time response was displayed within a resolution of $t = \pm 0.1$ sec ($t^* \leq \pm 3$).

3.3 Shear Flow Measrements

The extremely low speeds (0.0 to 0.4 m/sec) that were required to simulate the dense cloud drift necessitated the use of special calibration procedures for the hot wire anemometer used to measure velocities and turbulence. DISA 55A22 hot wires monitored by a DISA 55D01 anemometer were calibrated in a low-speed nozzle whose speed was set with low-volume flowrators. Velocity and turbulence measurements were made over the test section to detect the presence of any secondary cross currents. Velocities are reliable within 25%.

4.0 BEHAVIOR OF EXPERIMENTAL DATA

Experiments were performed with Freon-12 (Specific Gravity = 4.17 and a neutral density Helium/Freon-12 mixture (Specific Gravity $\simeq$ 1.0) and 35, 165, and 450 cm^3 initial volumes; hence length scales for the dense releases were L = 3.3, 5.5 and 7.7 cm; whereas time scales were T = .032, .042, and .049 seconds respectively. Wind tunnel velocities at a 10 cm reference height were varied from 0 to 1.0 m/sec.

4.1 Shear Flow Characteristics

Equilibrium boundary layers were developed over the last 3 meters of the test section. Velocity profiles were found to fit a power law exponent p = 0.13 above 1 cm and to fit a logarithmic velocity profile over most of the boundary layer with $u_*/u_R \simeq 0.048$ and $z_o = 2.4 \times 10^{-5}$ m. Characteristic Richardson numbers, $Ri_* = g_i' V_i^{1/3}/u_*^2$, varied from 445 to 26,000 and ∞ at calm conditions. Local longitudinal turbulence intensities were about 20% at the predominant cloud layer height of 0.5 cm. Shear stresses were nearly constant over dispersion depths, vertical turbulence intensities were small, ~ 6%. Evaluation of profile shape, turbulence intensities, and integral scales suggested the simulated boundary layer scale was between 1:1000 to 1:2000.

4.2 Dense Cloud Dispersion During Calms

Over the ten-fold range of source volumes studied all radial growth and concentration decay behavior collapsed together when plotted as R^* vs t_a^*, χ_m vs t_a^*, and χ_m vs R^*. The data also duplicated the earlier behavior of independent experiments performed by Lohmeyer et al. (1981) for 50 cm^3 source volumes released in a different wind tunnel using different instrumentation and release mechanism. Average data behavior are included with wind shear results discussed in the following paragraphs.

4.3 Dense Cloud Dispersion with Wind Shear

The presence of a wind field influences the dispersing dense gas in the following manner. In a weak or moderate wind the cloud slumps rapidly. It spreads radially, but the portion moving upwind slows somewhat and thickens. Subsequently, the entire cloud begins to drift downwind. When gravity driven velocities fall below local wind field speeds, at t^* near $Ri_* C_f/2$, background turbulence and wind shear begin to enhance entrainment, and when gravity driven velocities fall below u_* at $t^* \simeq Ri_*$, the shear flow completely dominates mixing.

Results from the experiments for varing wind shear are presented in Figures 2, 3, and 4. The downwind transport of a dense cloud in terms of dimensionless coordinates x^* and t_a^* is shown in Figure 2. One notes the regular decrease in cloud arrival time as u_R^* increases (as Ri_* decreases). The clouds appear to accelerate toward background advection speeds only after an initial inertial hesitation. The cloud appears to remain stationary for $t_a^* < 10$.

Figures 3 and 4 describe plume dilution χ_m versus t_a^* and x^* respectively. Plume concentrations decay assympototically as $(t_a^*)^{-3/2}$ and $(x^*)^{-3}$ during calm situations. For wind shear situations concentration variation with arrival time behaves in a rather irregular manner depending on initial cloud size. For the smallest cup size increasing wind speed results in progressively faster concentration decay rates. For the medium and large cup sizes small wind velocities result in apparently lower concentration decay rates, as the clouds are convected downwind without a proportionally higher rate of dilution. At higher wind speeds the cloud dilutes faster, the decay rate increases, and the slope of the χ_m vs t_a^* curves steepen again.

As shown in Figure 4 concentrations universally increase downwind with wind speed compared to the calm situation; however, the data suggests for each cloud size and downwind location a wind speed exists which results in maximum concentrations measured. At higher wind speeds one expects the added diluting capacity of the atmosphere to cause concentrations to vary inversely with wind speed for a fixed source rate.

Figure 5 emphasizes again the influence of wind shear by examining the variation of t_a^* and χ_m when x^* is held constant and the variation of χ_m when t_a^* is held constant. No strong source size perturbation is apparent in the distribution of arrival times; however, source size obviously influences concentrations at low wind speeds. As u_R^* becomes large χ_m appears to approach similar values for all source sizes studied at the given t_a^*.

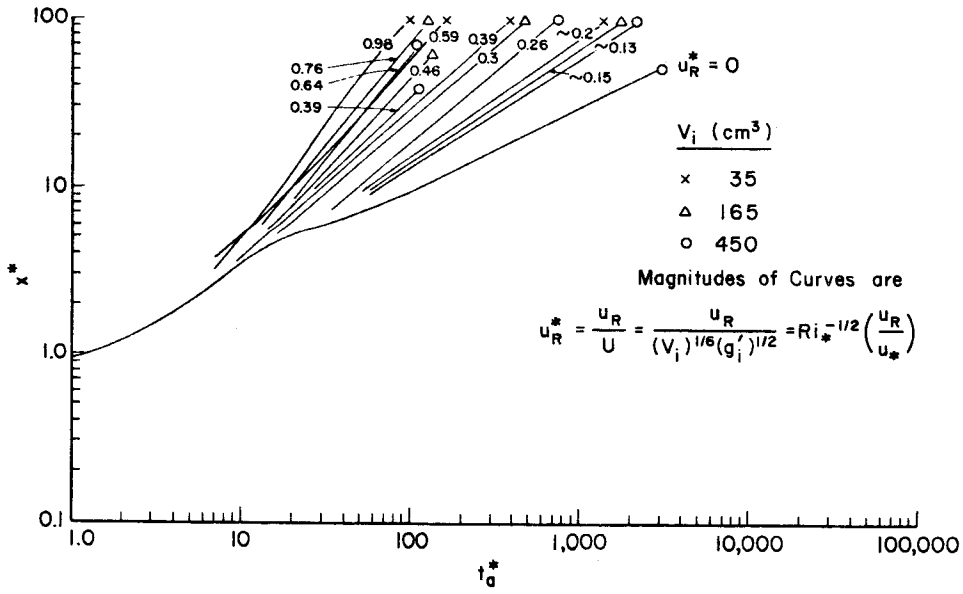

Figure 2. Cloud Transport Distance versus Arrival Time.

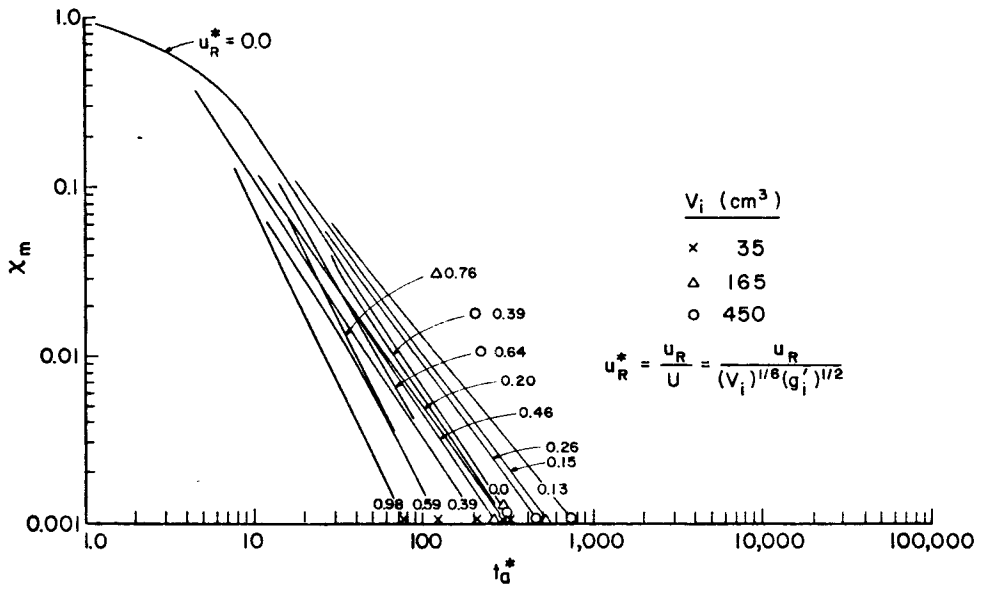

Figure 3. Cloud Dilution versus Arrival Time.

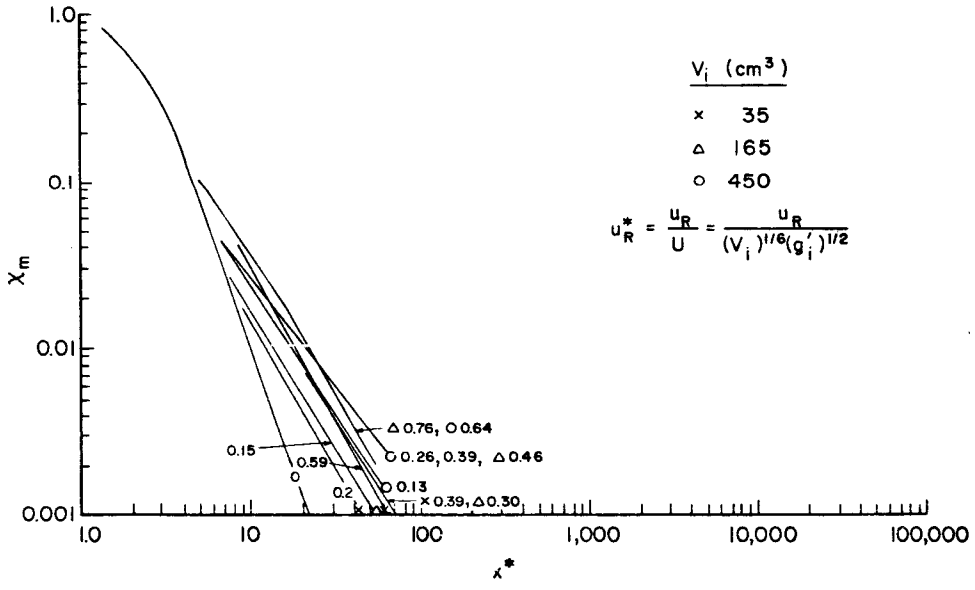

Figure 4. Cloud Dilution versus Downwind Distance.

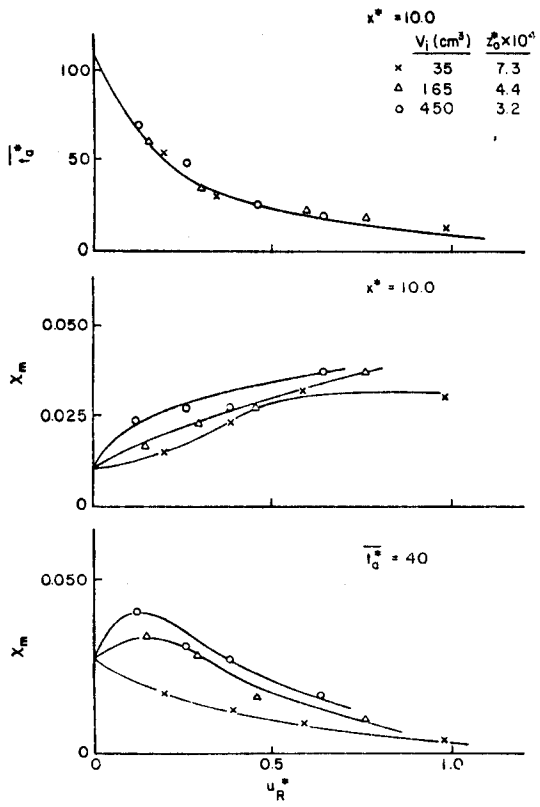

Figure 5. Variation of Arrival Time and Concentration with Velocity

5.0 BEHAVIOR OF NUMERICAL BOX MODEL

The volume-averaged box model discussed earlier can reproduce radial cloud dimensions and maximum concentrations measured during calm conditions within experimental error and statistical scatter. It can not reproduce the actual vertical and radial variations of height, concentration and velocity in time. Indeed, if the box model is designed to reproduce maximum concentrations measured at various radial locations, then the bulk average concentrations predicted will always be too low, and the entrainment rates too high for the reality of local entrainment physics. Nonetheless, such a model has engineering value and it is important to evaluate its limitations. Calculations of cloud transport distance and concentrations are plotted in Meroney and Lohmeyer (1982). Results are very similar with a few exceptions. Due to the well mixed cloud assumption the model can not reproduce the lower

decay rates at low wind speeds and higher decay rates at high wind speeds. The box model does reproduce the set of curves representative of greater mixing rates at faster wind speeds. It also predicts larger concentrations at a given distance for faster wind speeds. The limiting decay rates at low concentrations behave as $\chi_m \sim t_a^{*-1/3}$ and $\chi_m \sim x^{*-1/3}$ at larger times.

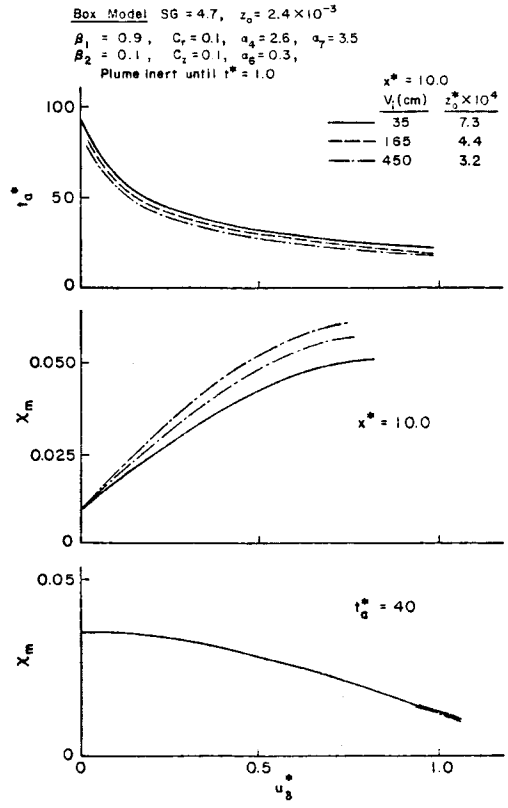

Figure 6. Variation of Arrival Time and Concentration with Velocity, Box Model Predictions.

To illuminate the independent effects of Ri_* and z_o^* the box model results were plotted as shown in Figure 6. Comparable data is found on Figure 5. The box model results are generally similar, but they do not reproduce the source size or roughness effect found in the plots

of dilution versus wind speed. Nonetheless, for such a simple model the predictions are respectable.

6.0 MODEL TO FIELD DATA COMPARISONS

Restricting attention to instantaneous spills of a fixed volume of heavy gas one finds field experiments performed on the sudden release of Freon-12 with an initial mixed specific gravity of 1.25, (Van Ulden, 1974), and spills of liquid natural gas (LNG) on land or water with initial specific gravities near 1.5 (AGA, (1974); Feldbauer et al., (1972); and Koopman, et al., (1982)). Most recently, Picknett (1978) describes the release of air/Freon gas mixtures with initial specific gravities ranging from 1.03 to 4.17. The LNG experiments are complicated by release mechanisms, and the recent Freon experiments may suffer from instrument placement problems, (Fay, 1980) and data inconsistencies (Hall, Hollis, and Ishaq, 1982). If we limit our attention to situations where releases are most nearly instantaneous (i.e. $t_{Release} \leq 5$) then only the Freon experiments of Picknett (1978) and Test No. 8 from the Burro China Lake LNG spill series are comparable to the box model considered herein.

6.1 Box Model Comparisons to Porton Downs Trials

The Porton Downs field trials used a gas source in the form of a cubical box of about 3.5 m side containing 40 m^3 of gas. The gas was released by allowing the sides of the box (made of thin pleated tarapulin material) to collapse to the ground under gravitational forces in about 0.8 seconds leaving a cube of the dense gas suddenly exposed to the prevailing wind conditions (Picknett, 1978). A total of 42 individual trials were run, covering a wide range of wind speeds, released gas density, surface roughness, atmospheric stability and ground slope. Measurements included visual records of plume outline as evidenced by

tracer smoke and dosage and continuous concentration monitors. The gases released were mixtures of Freon and air adjusted to specific gravities ranging from 1.2 to 4.2.

Hall, Hollis, and Ishaq (1982) reproduced the behavior of Runs 3, 8, 21, 29, 33, and 37 from the Porton trials in a set of wind-tunnel experiments. In all cases they reproduced the time variation of plume width, plume shape, plume arrival and plume departure very well. There were very strong visual similarities between the field and model plumes. Comparisons were also made between field concentration measurements and the model measurements. Some of the comparisons showed very good agreement, but others were poor. Differences were attributed to the naturally occurring high levels of repeat variability and anomalies in the field measurements. (In some cases the data from integrated continuous monitors and dosage monitors varied by more than an order of magnitude.)

These same situations were calculated by the box model. In each case the model replicated the Hall et. al. behavior quite well and differed from the field data in the same manner that their tests did. Porton Trial 8 results are shown in Figures 7, 8, 9. The field tests were performed at wind speeds below the threshhold values of the instruments available; hence the trial experiments were effectively in still air. Figure 7 displays peak gas concentrations measured at different downwind locations. Hall's model tests and the box model agree very well, but the field measurements do not seem to vary at all with distance. Figure 8 compares wind-tunnel, full scale, and box model cloud widths at various times from release. Agreement is excellent. Figure 9 displays concentration versus time traces at various radial locations. The box model predicts peak concentrations and arrival times very well.

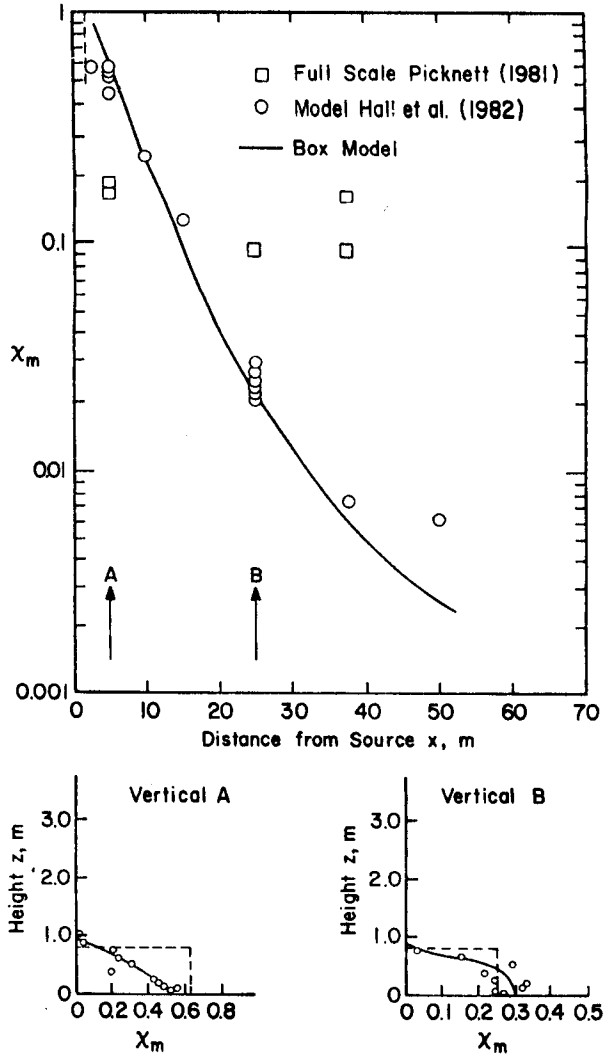

Figure 7. Porton Trial No. 8 - Peak Concentrations in Cloud

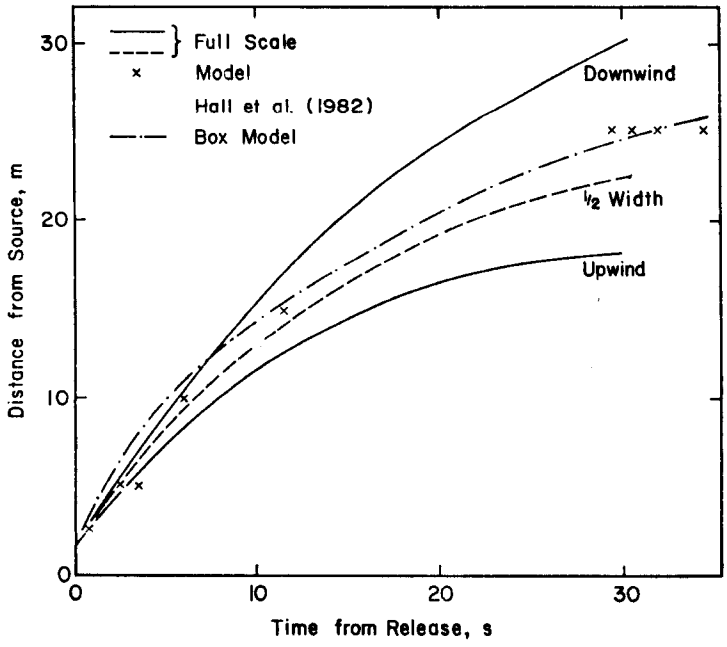

Figure 8. Porton Trial No. 8 - Cloud Size Variation

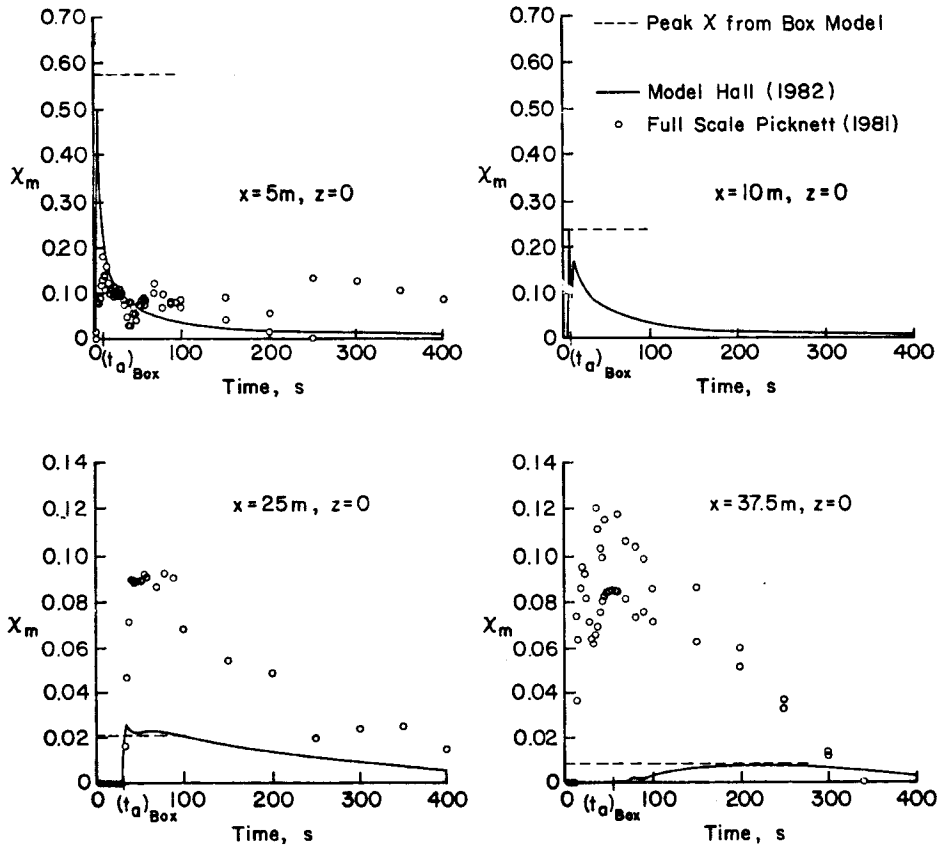

Figure 9. Porton Trial No. 8 - Continuous Monitor Measurements

6.2 Box Model Comparison to Burro No. 8 China Lake Trial

During the Burro 8 Field Trial at China Lake Naval Weapons Center 28.4 m^3 of LNG was released at a rate of 16.0 m^3/min onto a small water pond. The wind speed was 1.8 ± 0.3 m/sec and decreasing at 1 m height, while the atmospheric stability was slightly stable. Humidity was measured to be 5% upwind of the spill and air temperature was 33°C. * This spill displayed the most gravity dominated behavior of those performed. (See Koopman, et al. (1982), and Meroney and Neff (1981), for a discussion of field data.)

The box model described in Section 2.0 was run for Burro 8 initial conditions for a) adiabatic entrainment of dry air and b) mixed convec-

---

* Since the plume mixes violently over the pond it is likely that humidity downwind of the pond is higher (say 20%).

tion heat transfer and entrainment of air at 20% humidity. The maximum concentrations of methane, χ_m, versus downwind distance, x, is plotted in Figure 10. Both predictions are well within the scatter of the field data. Water vapor condensation and heat transfer initially result in somewhat accelerated dilution out to 150 m; however subsequent re-evaporation of condensed water vapor re-cools the plume and the two curves rejoin one-another. Although the effects of heat transfer and humidity are to accelerate entrainment, they also reduce the plumes lateral spread, (See Figure 11). This reduction of plume surface area seems to compensate for any increased entrainment rate; hence plume concentrations are only slightly modified by heat transport. Indeed one finds that the adiabatic plume calculation or an isothermal physical model simulation tend to be slightly conservative predictors for the real situation.

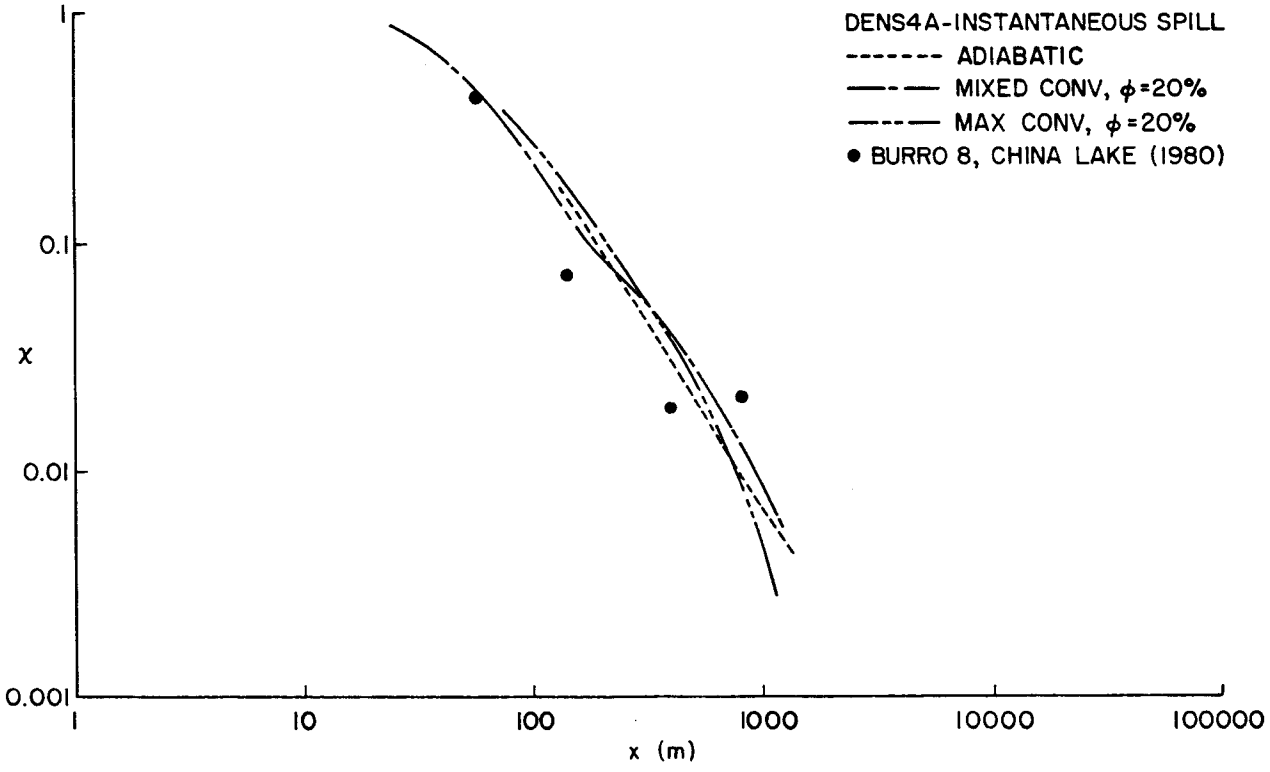

Figure 10. Burro Trial 8 Peak Concentrations at Ground Level vs. Downwind Distance

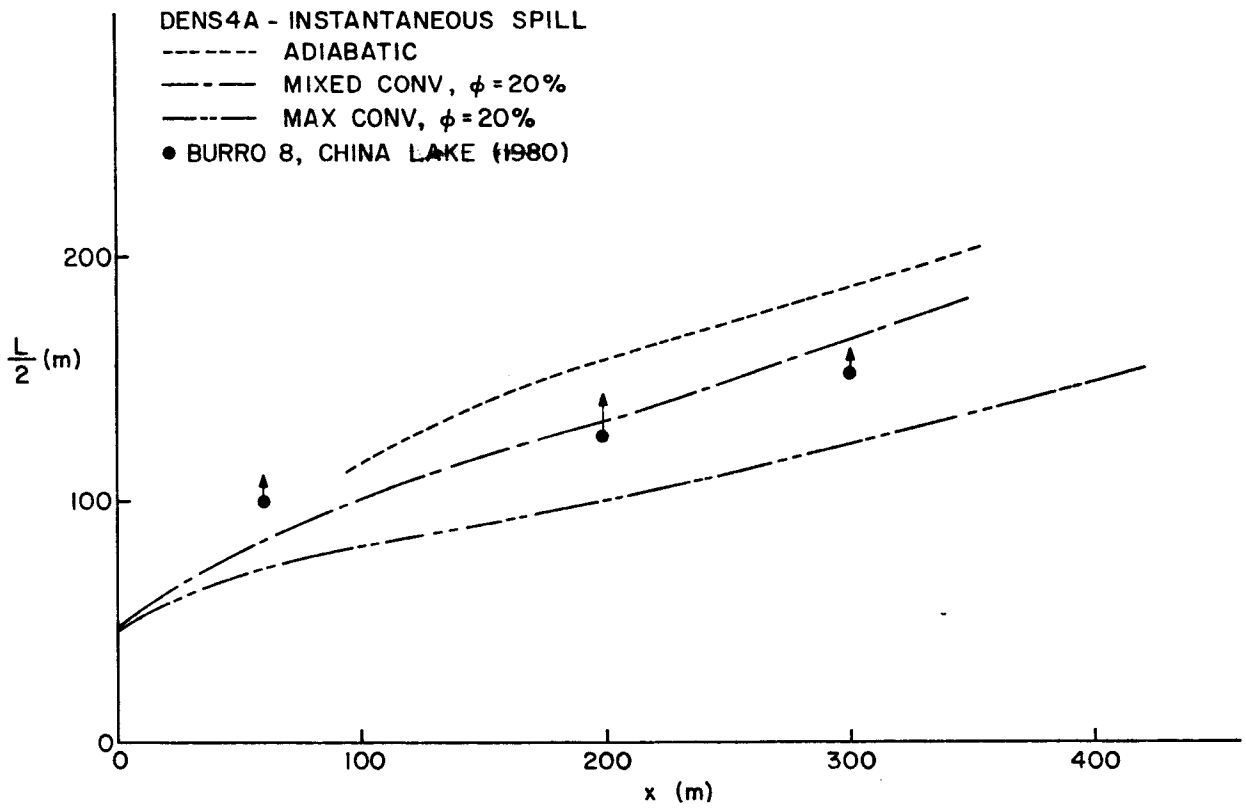

Figure 11. Burro Trial 8 Lateral Cloud Width vs. Downwind Distance

7.0 CONCLUSIONS

A series of experiments with sudden release of dense gas volumes at the ground in a shear flow confirms that inertial/buoyant spreading is rapidly followed by self generated entrainment. When Richardson numbers are sufficiently large, the gas may be diluted well below flammable or toxic limits before the effects of shear turbulence are evident. No previous numerical dense cloud model has been evaluated with respect to such a large set of controlled and repeated experiments.

ACKNOWLEDGEMENTS

The author wishes to acknowledge support from the Institute Wasserbau III, University of Karlsruhe, the von Humboldt Foundation, F.R.G., and the Gas Research Institute, U.S.A.

REFERENCES

American Gas Association (1974), LNG Safety, Program Interim Report on Phase II Work, AGA Project IS-3-1 Battelle, Columbus Laboratories.

Fay, J. A. (1980), Gravitational Spread and Dilution of Heavy Vapor Clouds, Second International Symposium on Stratified Flows, Trondheim, Norway, 24-27 June, pp. 421-494.

Feldbauer, G. F., Heigl, J., May, W. et al. (1972), Spills of LNG on Water-Vaporization and Downwind Drift of Combustible Mixture, Report No. ZE6IE-72, Esso Research and Engineering Co., Florham Park, New Jersey.

Hall, D. J., Hollis, E. J., and Ishaq, H. (1982), A Wind-Tunnel Model of the Porton Dense Gas Spill Field Trials, Warren Spring Laboratory, Department of Industry, Stevenage, U.K., Report L 394 (AP), 108 pp.

Koopman, R. P., Cederwall, R. T., Ermak, D. L., Goldwire, H. C. Jr., Hogan, W. J., McClure, J. W., McRae, T. G., Morgan, D. L., Rodean, H. C., and Shinn, J. H. (1982), Analysis of Burro Series 40 m^3 LNG Spill Experiments, J. of Hazardous Materials, Vol. 6, Nos. 1 and 2, pp. 43-84.

Lohmeyer, A., Meroney, R. N. and Plate, E. (1981), Model Investigations of the Spreading of Heavy Gases Released from an Instantaneous Volume Source at the Ground, Air Pollution Modeling and Its Applications, Vol. 1, C. de Wispelaere (Ed.), Plenum Publishing Corp., pp. 433-448.

Meroney, R. N. and Neff, D. E. (1980), Physical Modeling of Forty Cubic Meter LNG Spills at China Lake, California, Air Pollution Modeling and Its Applications, C. de Wispelaere (Ed.), Plenum Publishing Corp., pp. 24-27.

Meroney, R. N. and Lohmeyer, A. (1982), Gravity Spreading and Dispersion of Dense Gas Clouds Released Suddenly into a Turbulent Boundary Layer, Colorado State University Research Report CER82-83RNM-AL-7, Fort Collins, Colorado, Gas Research Institute Report 81/0025.

Meroney, R. N., Neff, D. E., and Cermak, J. E. (1978), Wind-Tunnel Modeling of LNG Spills, American Gas Association Transmission Conference, 8-10 May, Montreal, Canada, 26 pp.

Meroney, R. N. (1982), Wind-Tunnel Experiments on Dense Gas Dispersion, J. of Hazardous Materials, Vol. 6, Nos. 1 and 2, pp. 85-106.

Picknett, R. G. (1978), Fluid Experiments on the Behavior of Dense Clouds, Part I, Main Report, Ptn 1 L 1154/78/1, Chemical Defence Establishment, Porton Down, U.K.

Puttock, J. S., Blackmore, D. R., and Colenbrander, G. W. (1982), Field Experiments on Dense Gas Dispersion, J. of Hazardous Materials, Vol. 6, Nos. 1 and 2, pp. 13-42.

van Ulden, A. P. (1974), On the Spreading of a Heavy Gas Released Near the Ground, Proceedings of First International Loss Prevention Symposium, the Hague/Delft, Elsevier, Amsterdam, pp. 431-439.

van Ulden, A. P. (1979), The Unsteady Gravity Spread of a Dense Cloud in a Calm Environment, 10th International Technical Meeting on Air Pollution Modeling and Its Application, NATO-CCMS, Rome, Oct. 26, 9 pp.

NOTATIONS

Symbols	Definition
c_r, c_z	Entrainment coefficients
$C_f/2$	Skin friction coefficient
g_f	Modified gravitational constant
Gr	Grashof number, Eq. (13)
h_s	Surface heat transfer coefficient, Eq. (11)
H^s	Height of cloud
k	von Karman coefficient
L	Length scale
p	Power law coefficient
Pr	Prandtl number for air
R	Cloud radius
Re_*, Re	Reynolds number, Eq. (13)
Ri_*	Richardson number, Eq. (13)
t	Time
t_a	Cloud arrival time at x
T^a	Time scale
u	Gravitational spread velocity
u^g	Advection velocity
u^χ	Friction velocity
u_*	Cloud volume
V	Downwind distance
x	Roughness length
z_o	Various constants in Eqs. (1) to (6)
α_i, β_i	Plume dilution, volume or mole fraction
χ	Dimensionless source properties, Eq. (13)
s^*, Θ, β	Water vapor mass fraction in air
$\omega_{\phi,T}$	

Subscripts	
i	Initial cloud property
a	Property of ambient air
R	Evaluated at reference height (z_R = 10 cm)

Superscripts	
*	Nondimensional quantity